Relativistic fine-structure oscillator strengths for Li-like ions

L. Natarajan,[1] A. Natarajan,[2] and R. Kadrekar[1]
[1]*Department of physics, University of Mumbai, Mumbai 400032, India*
[2]*Department of physics, SIWS College, Wadala, Mumbai 400031, India*
(Received 14 October 2010; published 22 December 2010)

Relativistic configuration interaction results on the weighted oscillator strengths are presented for the Kβ satellite x rays from $1s2s3p$-$1s^22s$ transitions in Li-like ions with $14 \leqslant Z \leqslant 54$. The calculations are carried out in the active space approximation using multiconfiguration Dirac-Fock wave functions with the inclusion of the finite nuclear size effect, the Breit interaction, and quantum electrodynamic corrections. The resulting x-ray wavelengths and rates are compared with other available data. An attempt is also made to analyze the irregularities in the fine-structure energy levels and x-ray rates due to configuration mixing together with the Breit interaction.

DOI: 10.1103/PhysRevA.82.062514 PACS number(s): 32.30.−r, 31.15.−p

I. INTRODUCTION

The x rays emitted from highly ionized few-electron atoms are proved to be important in determining the various plasma parameters [1–4]. Accurate x-ray energies and rates from few-electron ions have been measured in laser-produced plasmas [5], tokomak plasmas [6–10], and beam-foil spectroscopy [11–13] and ion-atom traps [14]. Systematic relativistic and nonrelativistic calculations on the isoelectronic sequence of Li-like ions have been the subject of several studies in the past. The experimental observations on the Kβ spectrum of He-, Li-, and Be-like iron from tokomak fusion test reactor (TFTR) plasmas along with the data from the HULLAC package have been reported by Smith *et al.* [8]. Similar theoretical results and experimental investigations on argon recorded with a high-resolution spectrometer on the Princeton Large Torus tokomak plasmas have been analyzed by Beiersdorfer *et al.* [9]. The x-ray spectra of He-like mid-Z ions and their associated dielectronic satellite emission have been observed with a high-resolution crystal spectrometer at the Lawrence Livermore electron-beam ion trap (EBIT) by Smith *et al.* [14]. The possibility of overlap between the Kβ x-rays from Li-like Al and L x-rays from Ne-like Rb has been experimentally observed by Elliott *et al.* [15]. The synthetic x-ray satellite lines from Li-like Si have been compared with the solar flare spectra by Phillips *et al.* [16]. The MZ calculations, based on the Z-expansion method, on the relative intensities of dielectronic satellite lines from $1s2l''nl'$-$1s^2n'l'(n,n' = 2,3)$ have been reported by Safronova *et al.* [17] for a wide range of Z. The dielectronic satellite spectra involving x-ray and Auger transitions in He-, Li-, and Be-like ions have been studied by Chen [18] using multiconfiguration Dirac-Fock (MCDF) wave functions with the inclusion of generalized Breit interaction and quantum electrodynamic corrections. Recently, extensive tabulations on the x-ray energies and rates for various transitions from $n = 2$ and 3 to $n = 1$ and the autoionization rates for doubly excited $2lnl'$ and $1s2lnl'$ states in ions with atomic numbers $Z = 6$ to 36 have been reported by Goryayev *et al.* [19]. The calculations were carried out by them using MZ code with the inclusion of relativistic corrections within the framework of the Breit operator. However, detailed analysis of the characteristics of the transition rates from few-electron ions has not been carried out. The purpose of the present work is to mainly analyze the effects of correlation and the Breit interaction on the Kβ x-ray satellites from $1s2s3p$ configurations in Li-like ions.

In this article the x-ray energies and rates from $1s2s3p$-$1s^22s$ transitions are analyzed using MCDF wave functions with the inclusion of the Breit interaction, self-energy, and vacuum polarization. The finite nuclear size effect has been included in the calculations by considering a two-parameter Fermi charge distribution. The MCDF method is shown to be efficient in treating the correlation effects due to strong interaction of the nearly degenerate excited states with the reference state [20,21]. The correlation effects have been computed by excitation of atomic orbitals in the active space approximation. The calculations have been carried out using the GRASP2K code [22,23] for Li-like isoelectronic sequence in the range $Z = 14$ to 54.

II. NUMERICAL PROCEDURE

In a multiconfiguration relativistic calculation, the configuration state functions (CSFs) are antisymmetrized sum of product of Dirac spinors and the atomic state function (ASF) is expanded in terms of CSFs.

$$\Psi(\gamma\, P\, J\, M) = \sum c_{it}\varphi_i(\gamma_i\; P\, J\, M) \tag{1}$$

where c_{it} are the mixing coefficients for the state i and the summation runs over all the CSFs included in the evaluation of ASF. The configuration mixing coefficients are obtained through the diagonalization of the Dirac-Coulomb Hamiltonian

$$H_{\mathrm{DC}} = \sum_i \left[c\bar{\alpha}_i \cdot \bar{p}_i + (\beta_i - 1)c^2 - \frac{Z}{r_i} \right] + \sum_{i>j} \frac{1}{r i_j} \tag{2}$$

Once a set of radial orbitals and the expansion coefficients are optimized for self-consistency, RCI calculations can be performed by including higher-order interactions in the Hamiltonian. The most important of these are the transverse photon interaction, self-energy, and vacuum polarization corrections. The Dirac spinors and the expansion coefficients are described in detail in the literature [24,25]. The theoretical background necessary for the evaluation of x-ray energies and rates using

MCDF wave functions including higher-order correction terms is described by many in the past [24–26].

The construction of near exact atomic state functions using systematic expansion of the orbitals in the active space and the effects of the various orbitals on the transition rates have been discussed in detail in our earlier studies [20,21], [27,28]. In this work, the zero-order Dirac-Fock (DF) wave functions were generated from the $1s2s3p$ and $1s^22s$ reference configurations in extended optimal level (EOL) scheme where the radial orbitals and the mixing coefficients are determined by optimizing the energy functional which is the weighted sum of the energy values corresponding to a set of eigenstates. The succeeding terms were obtained by considering an active space in which the *jj*-coupled CSFs of a given parity P and J symmetry are generated by excitation of electrons from the reference configuration to the orbitals in the active set. We first evaluated the single configuration DF energies and rates of the Kβ satellites without taking into account correlation effects and higher-order corrections. We then generated 24 CSFs based on the four relativistic subshells in the reference configurations by considering single and double (SD) excitations of electrons and evaluated the transition energies and rates. By gradually expanding the size of the active space, two sets of calculations, one with only correlation effects (MCDF) and the other with the Breit interaction and QED corrections coupled with correlation functions known as relativistic configuration interaction (RCI), were repeated for each step by step multiconfiguration expansion, taking care of the convergence criteria which in this work was taken to be 10^{-8}. As the orbital set generated from the SD excitations of electrons in the reference sushells were found to be better optimized than monoconfiguration functions, our entire analysis on the effects of large configuration mixing together with Breit interaction is carried out with respect to this limited reference set.

The active set considered in this work consisted of relativistic subshells with the principal quantum number $n \leqslant 7$. The set consisting of all CSFs with the same n and same parity is referred to as Layzer complex [22]. The $n = 1$ to 6 Layzer complex consisted of $l = 0$ to 3 spin orbitals while for the $n = 7$ Layzer we considered only spin orbitals with $l \leqslant 2$. Further expansion of the active space did not contribute much to the mixing coefficients and we expect that the above active set takes into account all the important correlation configurations.

III. RESULTS AND DISCUSSION

The energy levels can be classified without ambiguity in the LS and *jj*-coupling schemes for low- and high-Z elements, respectively. However for intermediate values of Z, neither of these notations provide a correct representation and hence our present usage of energy ordering to identify the low-lying states from relativistic computation in simple LSJ designations cannot be taken as a proper spectroscopic classification.

It is observed that the fine structure levels of ions with $Z =$ 14 to 46 with limited correlations (24 CSFs) follow the level structure $^4P_{1/2}, ^4P_{3/2}, ^4P_{5/2}, (^3S_1)^2P_{3/2}, (^3S_1)^2P_{1/2}, (^1S_0)^2P_{1/2}$, and $(^1S_0)^2P_{3/2}$ arranged respectively in decreasing order of negative energies. Our calculations show that influence of neither large correlations with more than 4000 CSFs nor higher-order corrections alters the limited correlation level scheme of ions with $Z < 30$ and hence adheres to the above LSJ energy level scheme. However, both these effects affect the fine-structure levels of ions in the range $Z = 30$ to 38 and cancel each other, thereby bringing back the expected LSJ structure. For these ions, the MCDF energy of $(^3S_1)^2P_{1/2}$ state becomes slightly more bound than $(^3S_1)^2P_{3/2}$ state due to large configuration mixing. The first two major contributing configurations to these states are the same as they are for $Z < 30$. However, although the other CSFs contributing to the mixing coefficients also remain the same, the weight of the contribution from these CSFs varies and this leads to a flip in the level structure. For example, for $Z = 28$ and 36, the significant correlation configurations to the $(^3S_1)^2P_{1/2}$ state are $1s2s(^3S_1)3p_{3/2}$, $1s2p_{1/2}(^3P_0)3s$, $1s2p_{3/2}(^3P_1)3s$, $1s2p_{1/2}(^1P_1)3s$, and $1s2s(^1S_0)3p_{1/2}$. While the maximum contribution comes from the admixture of first two CSFs for both these ions, the third contribution is from $1s2p_{3/2}(^3P_1)3s$ for $Z = 28$, whereas it is from $1s2s(^1S_0)3p_{1/2}$ for $Z =$ 36. Similarly for the $(^3S_1)^2P_{3/2}$ state, the two main CSFs, $1s2s(^3S_1)3p_{3/2}$ and $1s2p_{1/2}(^1P_1)3s$, are the same for both $Z = 28$ and 36. While the next contribution for $Z = 28$ is from $1s2s(^3S_1)3p_{1/2}$, it is from $1s2s(^1S_0)3p_{3/2}$ for $Z = 36$. Such admixtures lead to the inversion of $(^3S_1)^2P_{3/2}$ and $(^3S_1)^2P_{1/2}$ states for these ions. It is also observed that due to the large correlation effect, the $(^3S_1)^2P_{1/2}$ state becomes more bound than the $^4P_{5/2}$ state as a result of which these two states get inverted. However, contributions from the Breit interaction

TABLE I. Sample data on fine structure energy levels from $1s2s3p$ configuration in Li-like ions showing the influence of correlation and Breit + QED corrections on the level structure.

Z	24 CSFs	3993 CSFs	Breit + QED
36	$(^1S_0)^2P_{3/2}$	$(^1S_0)^2P_{3/2}$	$(^1S_0)^2P_{3/2}$
	$(^1S_0)^2P_{1/2}$	$(^1S_0)^2P_{1/2}$	$(^1S_0)^2P_{1/2}$
	$(^3S_1)^2P_{1/2}$	$(^3S_1)^2P_{3/2}$	$(^3S_1)^2P_{1/2}$
	$(^3S_1)^2P_{3/2}$	$^4P_{5/2}$	$(^3S_1)^2P_{3/2}$
	$^4P_{5/2}$	$(^3S_1)^2P_{1/2}$	$^4P_{5/2}$
	$^4P_{3/2}$	$^4P_{3/2}$	$^4P_{3/2}$
	$^4P_{1/2}$	$^4P_{1/2}$	$^4P_{1/2}$
42	$(^1S_0)^2P_{3/2}$	$(^1S_0)^2P_{3/2}$	$(^1S_0)^2P_{3/2}$
	$(^1S_0)^2P_{1/2}$	$(^1S_0)^2P_{1/2}$	$(^3S_1)^2P_{1/2}$
	$(^3S_1)^2P_{1/2}$	$(^3S_1)^2P_{1/2}$	$(^1S_0)^2P_{1/2}$
	$(^3S_1)^2P_{3/2}$	$^4P_{5/2}$	$^4P_{5/2}$
	$^4P_{5/2}$	$(^3S_1)^2P_{3/2}$	$(^3S_1)^2P_{3/2}$
	$^4P_{3/2}$	$^4P_{3/2}$	$^4P_{3/2}$
	$^4P_{1/2}$	$^4P_{1/2}$	$^4P_{1/2}$
54	$(^1S_0)^2P_{3/2}$	$(^1S_0)^2P_{3/2}$	$(^1S_0)^2P_{3/2}$
	$(^3S_1)^2P_{1/2}$	$(^3S_1)^2P_{1/2}$	$(^3S_1)^2P_{1/2}$
	$(^3S_1)^2P_{3/2}$	$(^3S_1)^2P_{3/2}$	$(^3S_1)^2P_{3/2}$
	$^4P_{5/2}$	$^4P_{5/2}$	$^4P_{5/2}$
	$(^1S_0)^2P_{1/2}$	$(^1S_0)^2P_{1//2}$	$(^1S_0)^2P_{1/2}$
	$^4P_{3/2}$	$^4P_{3/2}$	$^4P_{1/2}$
	$^4P_{1/2}$	$^4P_{1/2}$	$^4P_{3/2}$

TABLE II. A comparison of the present RCI x-ray wavelengths (Å) for $1s2s3p$-$1s^22s$ transitions in Li-like ions with other experimental and theoretical data.[a]

		$1s2s(^3S_1)3p$		$1s2s(^1S_0)3p$		$1s2s(^3S_1)3p$	
Z		$^2P_{1/2}$	$^2P_{3/2}$	$^2P_{1/2}$	$^2P_{3/2}$	$^4P_{1/2}$	$^4P_{3/2}$
14	A	5.8074	5.8076	5.7720	5.7712	5.8103	5.8101
	B	5.8083	5.8085	5.7741	5.7733	5.8113	5.8112
	C	5.8069	5.8071	5.7709	5.7701	5.8086	5.8084
	D	5.809	5.809	5.773	5.772	5.812	5.812
16	A	4.3825	4.3828	4.3592	4.3584	4.3848	4.3847
	C	4.3822	4.3824	4.3585	4.3577	4.3838	4.3837
18	A	3.4260	3.4262	3.4096	3.4081	3.4285	3.4282
	B	3.4236	3.4238	3.4079	3.4070	3.4255	3.4254
	C	3.4231	3.4233	3.4068	3.4059	3.4246	3.4245
20	A	2.7482	2.7484	2.7365	2.7351	2.7503	2.7501
	C	2.7468	2.7469	2.7351	2.7342	2.7482	2.7481
22	A	2.2533	2.2535	2.2448	2.2434	2.2552	2.2550
	B	2.2523	2.2525	2.2440	2.2430	2.2538	2.2537
	C	2.2521	2.2522	2.2435	2.2425	2.2534	2.2533
24	A	1.8800	1.8802	1.8736	1.8722	1.8817	1.8816
	C	1.8794	1.8795	1.8729	1.8718	1.8806	1.8805
26	A	1.5917	1.5918	1.5868	1.5857	1.5930	1.5929
	B	1.5917	1.5918	1.5869	1.5858	1.5930	1.5929
	C	1.5915	1.5916	1.5866	1.5855	1.5928	1.5927
	E			1.5868$^{\text{expt}}$	1.5855$^{\text{expt}}$		
	E	1.5912$^{\text{theory}}$			1.5853$^{\text{theory}}$		
28	A	1.3648	1.3649	1.3610	1.3599	1.3660	1.3659
	B	1.3647	1.3648	1.3608	1.3598	1.3659	1.3658
32	A	1.0346	1.0347	1.0323	1.0312	1.0358	1.0357
	C	1.0345	1.0346	1.0321	1.0310	1.0356	1.0355
34	A	0.9123	0.9124	0.9105	0.9094	0.9132	0.9134
	C	0.9122	0.9122	0.9103	0.9093	0.9132	0.9132
36	A	0.8102	0.8103	0.8088	0.8077	0.8113	0.8113
	B	0.8102	0.8103	0.8088	0.8077	0.8113	0.8112
	C	0.8101	0.8102	0.8086	0.8076	0.8112	0.8111
40	A	0.6505	0.6509	0.6499	0.6488	0.6518	0.6518
42	A	0.5877	0.5880	0.5872	0.5861	0.5889	0.5889
	B	0.5877	0.5874	0.5872	0.5861	0.5889	0.5888
44	A	0.5328	0.5331	0.5330	0.5319	0.5345	0.5344
48	A	0.4442	0.4443	0.4444	0.4433	0.4456	0.4456
50	A	0.4077	0.4078	0.4080	0.4069	0.4090	0.4090
52	A	0.3753	0.3754	0.3757	0.3746	0.3766	0.3766
54	A	0.3466	0.3467	0.3470	0.3459	0.3479	0.3479

[a]Abbreviations: A, present values; B, Ref. [18]; C, Ref. [19]; D, Ref. [16]; E, Ref. [8].

bring back the same limited configuration ordering of levels as observed for ions with $Z < 30$.

For ions in the range $Z = 39$ to 43, correlation and higher-order corrections flip the level scheme, thereby resulting in an anomalous structure. With large configuration mixing, it is observed that for ions with $Z \leqslant 38$, the main CSFs contributing to the $(^1S_0)^2P_{1/2}$ state in the decreasing order of mixing are $1s2s(^1S_0)3p_{1/2}$, $1s2p_{1/2}(^1P_1)3s$, $1s2s(^3S_1)3p_{3/2}$, and $1s2p_{3/2}(^3P_1)3s$. However, this sequence changes for ions in the range $Z = 39$ to 43. Considering $Z = 40$ and 42 as sample cases, we find that for the $(^1S_0)^2P_{1/2}$ state of $Z = 40$, the strong mixing is between $1s2s(^1S_0)3p_{1/2}$ (87%), $1s2s(^3S_1)3p_{3/2}$ (8.8%), $1s2p_{1/2}(^1P_1)3s$, and $1s2p_{1/2}(^1P_1)3d_{3/2}$ configurations. Also, the contribution to the $(^3S_1)^2P_{1/2}$ state from the expected $1s2s(^3S_1)3p_{3/2}$ decreases to 37%, whereas the maximum contribution comes from $1s2p_{1/2}(^1P_1)3s$ (42%) and the other significant contributions are from the $1s2p_{1/2}(^3P_0)3s$ (17%) and $1s2p_{3/2}(^3P_1)3s$ (2.5%) configurations. The net result of such an admixture leads to shuffling of the three $J = 1/2$ states in the normal energy level scheme. Also, the correlation contribution makes the $(^3S_1)^2P_{3/2}$ state more bound than the $^4P_{5/2}$ state. Although the influence of the Breit interaction on the level energies and transition rates is appreciable, it does not change MCDF ordering of the states.

For $Z = 42$, the mixing coefficients for $(^3S_1)^2P_{1/2}$ states in the decreasing mixing strength are from $1s2p_{1/2}(^1P_1)3s(50\%)$, $1s2s(^3S_1)3p_{3/2}(38\%)$, $1s2p_{1/2}(^3P_0)3s(8\%)$, $1s2p_{3/2}(^3P_1)3s(2\%)$, and $1s2s(^1S_0)3p_{1/2}$ (1.8%). Similar admixtures are found for the $(^3S_1)^2P_{3/2}$ state from

TABLE III. RCI rates (per second) of Kβ satellites for various fine-structure transitions from the $1s2s3p$ configuration in Li-like ions.[a,b]

		$1s2s(^3S_1)3p$		$1s2s(^1S_0)3p$		$1s2s(^3S_1)3p$	
Z		$^2P_{1/2}$	$^2P_{3/2}$	$^2P_{1/2}$	$^2P_{3/2}$	$^4P_{1/2}$	$^4P_{3/2}$
14	A	0.525(13)	0.52(13)	0.381(13)	0.369(13)	4.22(10)	1.712(11)
	B	0.49(13)	0.49(13)	0.425(13)	0.417(13)	3.45(10)	1.33(11)
	C	0.473(13)	0.437(13)	0.41(13)	0.408(13)	11.7(10)	5.40(11)
16	A	0.921(13)	0.897(13)	0.691(13)	0.657(13)	1.27(11)	0.551(12)
	C	0.843(13)	0.771(13)	0.738(13)	0.715(13)	2.41(11)	1.12(12)
18	A	1.72(13)	1.58(13)	1.49(13)	1.41(13)	5.90(11)	2.71(12)
	B	1.43(13)	1.37(13)	1.23(13)	1.17(13)	2.83(11)	1.24(12)
	C	1.40(13)	1.25(13)	1.22(13)	1.16(13)	4.81(11)	2.15(12)
20	A	2.68(13)	2.42(13)	2.47(13)	2.27(13)	1.06(12)	5.01(12)
	C	2.18(13)	1.92(13)	1.91(13)	1.75(13)	9.04(11)	4.26(12)
22	A	3.82(13)	3.37(13)	3.38(13)	3.04(13)	1.79(12)	8.59(12)
	B	3.30(13)	2.99(13)	2.84(13)	2.49(13)	1.23(12)	5.76(12)
	C	3.26(13)	2.81(13)	2.51(13)	2.85(13)	1.60(12)	7.58(12)
24	A	5.44(13)	4.66(13)	5.05(13)	4.31(13)	2.97(12)	1.44(13)
	C	4.68(13)	3.94(13)	4.10(13)	3.44(13)	2.67(12)	1.27(13)
26	A	6.62(13)	5.62(13)	5.48(13)	4.23(13)	3.88(12)	1.88(13)
	B	6.48(13)	5.49(13)	5.62(13)	4.41(13)	3.70(12)	1.76(13)
	C	6.50(13)	5.34(13)	5.74(13)	4.54(13)	4.27(12)	2.02(13)
28	A	8.79(13)	7.26(13)	7.50(13)	5.45(13)	6.08(12)	2.93(13)
	C	8.75(13)	7.02(13)	7.85(13)	5.84(13)	6.54(12)	3.08(13)
32	A	14.11(13)	11.11(13)	13.45(13)	8.63(13)	1.32(13)	6.20(13)
	C	14.5(13)	11.2(13)	14.1(13)	9.26(13)	1.39(13)	6.42(13)
34	A	16.9(13)	13.1(13)	17.8(13)	10.7(13)	1.84(13)	8.56(13)
	C	17.8(13)	13.4(13)	18.7(13)	11.5(13)	1.94(13)	8.86(13)
36	A	19.3 (13)	14.7(13)	23.8(13)	13.22(13)	2.52(13)	11.5(13)
	B	19.4(13)	14.5(13)	23.3(13)	13.3(13)	2.49(13)	11.2(13)
	C	20.9 (13)	15.6(13)	24.7(13)	14.3(13)	2.65(13)	11.9(13)
40	A	9.85(13)	14.85(13)	41.6(13)	19.66(13)	4.38(13)	1.93(14)
42	A	13.9(13)	30.2(13)	53.2(13)	23.8(13)	5.62(13)	24.4(13)
	B	50.8(13)	24.1(13)	14.1(13)	30.4(13)	5.65(13)	21.4(13)
44	A	17.3(13)	41.9(13)	62.5(13)	28.6(13)	7.09(13)	30.4(13)
48	A	69.5(13)	67.3(13)	67.7(13)	40.5(13)	10.9(13)	45.3(13)
50	A	100.1(13)	80.7(13)	69.1(13)	47.8(13)	13.2(13)	54.4(13)
52	A	130.7(13)	95.1(13)	71.6(13)	55.9(13)	15.9(13)	64.7(13)
54	A	166.7(13)	115.4(13)	81.1(13)	68.8(13)	19.8(13)	78.9(13)

[a]The number inside the parentheses is in powers of 10. Also included are the other relativistic rates.
[b]Abbreviations: A, present rates, B, MCDF Ref. [18]; C, MZ Ref. [19].

$1s2p_{1/2}(^1P_1)3s(52\%)$ and $1s2s(^3S_1)3p_{3/2}(46\%)$. Just like the changes observed in the sequence of mixing coefficients to the $(^1S_0)^2P_{1/2}$ state of $Z=40$, it is also seen that for $Z=42$ the maximum admixture is between $1s2s(^1S_0)3p_{1/2}(90\%)$ and $1s2s(^3S_1)3p_{3/2}(9\%)$. Also, as was noted for $Z=40$, the correlation flips the $(^3S_1)^2P_{3/2}$ and $^4P_{5/2}$ states. Although the other fine-structure states retain the same structure as was observed with a limited correlation, such strong admixtures significantly alter the transition rates from the $(^3S_1)^2P_{1/2}$,$(^3S_1)^2P_{3/2}$, and $(^1S_0)^2P_{1/2}$ states. However, the Breit interaction shuffles the three $J=1/2$ states and also affects considerably the x–ray rates. We note that a look at the mixing coefficients of the various states becomes necessary to make proper transition assignments for these ions.

For $Z=44$, with a limited correlation, the maximum contributions to the $(^1S_0)^2P_{1/2}$ state are from $1s2s(^1S_0)3p_{1/2}(65.7\%)$ and $1s2s(^3S_1)3p_{3/2}(33\%)$, whereas with a large correlation, the contributions from these CSFs are 89% and 7.5%, respectively. Similarly, the significant contributions to the $(^3S_1)^2P_{1/2}$ state with limited CSFs are from $1s2s(^3S_1)3p_{3/2}(67\%)$ and $1s2s(^1S_0)3p_{1/2}(32.7\%)$ while the major contributing CSFs from the large admixture turn out to be $1s2s(^3S_1)3p_{3/2}(46\%)$ and $1s2p_{1/2}(^1P_1)3s(36.6\%)$. We also observed similar changes between limited and the large correlation admixture for the $(^3S_1)^2P_{3/2}$ state. It is thus seen that such changes in the mixing coefficients from the extended CSF set makes the $(^1S_0)^2P_{1/2}$ state more bound than the $(^3S_1)^2P_{1/2}$and $(^3S_1)^2P_{3/2}$states. However, the contributions from the Breit interaction inverts the $(^1S_0)^2P_{1/2}$ and $(^3S_1)^2P_{3/2}$states, with the latter becoming slightly more bound than the former.

For $Z>44$, we observe that even with limited configuration functions, the so-far-observed level scheme with 24 CSFs is no more retained as the $(^1S_0)^2P_{1/2}$state is pushed down in the level structure. Its energy is more negative than

$(^3S_1)^2P_{3/2}$,$(^3S_1)^2P_{1/2}$,$^4P_{5/2}$, and $(^1S_0)^2P_{3/2}$. We note that a large correlation does not affect the limited configuration level scheme. However, the contribution from the Breit interaction to the mixing coefficients is seen to flip some of the states.

In Table I, sample data on the effects of additional configuration interaction and higher-order corrections on the energies of the various states from $1s2s3p$ configuration are given. The first column of the table gives the symbolic LSJ ordering of the states with 24 CSFs from the four relativistic orbitals in the reference configurations, column 2 gives contributions from 3993 CSFs, and column 3 lists the influence of large correlation coupled with higher-order relativistic corrections. The fine-structure states are grouped in the increasing order of negative energy in accordance with the standard energy level diagram description. The clear-cut identification of the spectra becomes complicated for $Z = 42$ due to anomalous mixing coefficients.

The RCI wavelengths of the Kβ x-rays from states of $1s2s3p$ configuration of ions in the range $Z = 14$ to 54 are listed in Table II. The available experimental energies [8] along with the relativistic data reported in Refs. [8,16,18,19] are included in the table. We have also made a detailed comparison of our data with the wavelengths tabulated by Goryayev *et al.* [19] using relativistic MZ expansion method and the MCDF extended average level (EAL) values of Chen [18]. The present wavelengths for Fe agree well with the experimental energies of Smith *et al.* [8] and their HULLAC code relativistic data for two transition from $1s2s3p_{3/2-}$ configuration. Our calculated wavelengths for Si are in good agreement with the synthetic spectra obtained by Phillips *et al.* [16]. Our computed energies are in general slightly less than EAL values of Chen [18] and marginally more than the MZ energies of Goryayev *et al.* [19] for small Z. However, for $Z > 24$, our energies are in excellent agreement with the EAL [18] and MZ [19] energies.

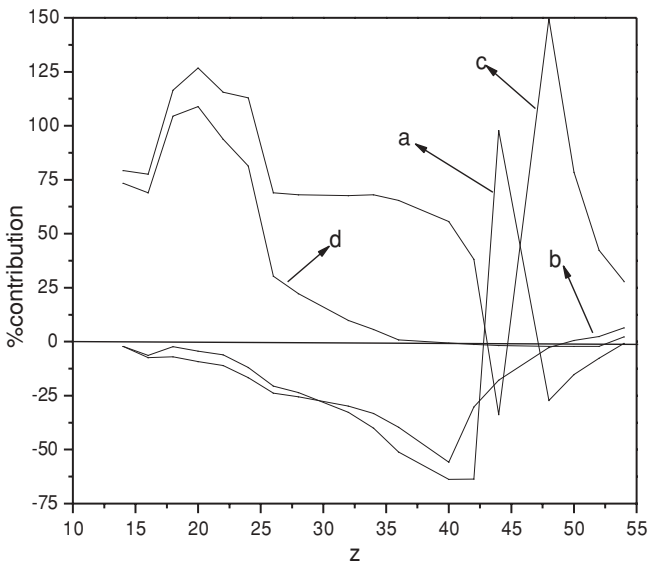

FIG. 1. Contribution from large configuration interactions to the allowed transition rates. The curves a, b, c, and d represent transitions to $1s^22s^2S_{1/2}$ state from $1s2s(^3S_1)3p^2P_{1/2}$, $1s2s(^3S_1)3p^2P_{3/2}$, $1s2s(^1S_0)3p^2P_{1/2}$ and $1s2s(^1S_0)3p^2P_{3/2}$ states, respectively.

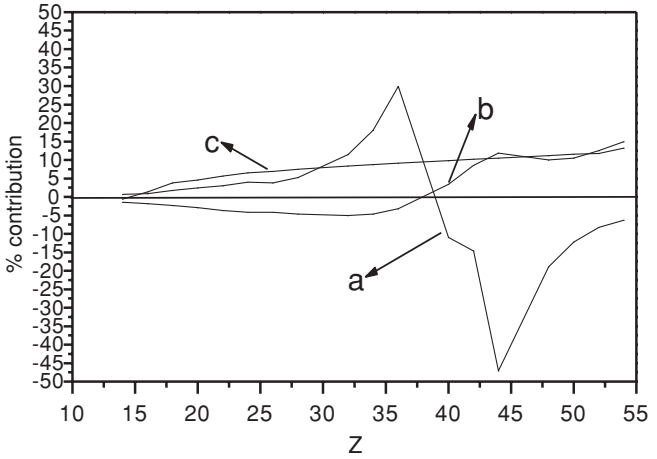

FIG. 2. Percentage contribution from Breit interaction to the transition rates. The transitions are from initial $J = 1/2$ to final $J = 1/2$ states. The curves a, b, and c represent transitions from $1s2s(^3S_1)3p^2P_{1/2}$, $1s2s(^1S_0)3p^2P_{1/2}$, and $1s2s(^3S_1)3p^4P_{1/2}$ states, respectively.

Our calculations show that the dipole rates for various transitions calculated in length and velocity forms are nearly the same for the allowed transitions and differ by a maximum of 3% for the forbidden transition. In Table III, we give our RCI length gauge rates along with earlier relativistic data [16–19]. Our comparison shows that for $Z < 26$, the present rates in general deviate slightly from the MCDF [18] and MZ [19] rates and are in good agreement with earlier rates for $Z > 26$. The EOL scheme adopted in this work along with large correlation configurations account for the small differences between our and earlier rates. For $Z = 42$, our RCI rates for $(^3S_1)^2P_{1/2-}{}^2S_{1/2}$ and $(^1S_0)^2P_{1/2-}{}^2S_{1/2}$ transitions are 13.9×10^{13} s^{-1} and 53.2×10^{13} s^{-1}, respectively, whereas the MCDF rates of Chen for these two respective transitions are 50.8×10^{13} s^{-1} and 14.1×10^{13} s^{-1} Similarly our rates for the $(^3S_1)^2P_{3/2-}{}^2S_{1/2}$ and $(^1S_0)^2P_{3/2-}{}^2S_{1/2}$ transitions are 30.2×10^{13} s^{-1} and 23.8×10^{13} s^{-1}, respectively, while the rates quoted by Chen [18] for these transitions are 24.1×10^{13} s^{-1}

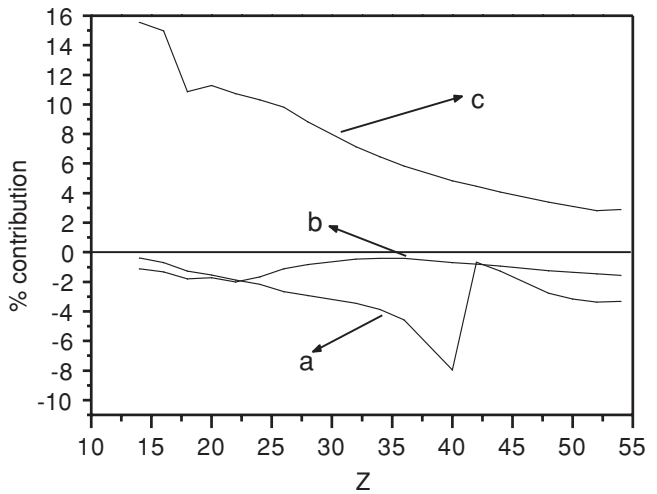

FIG. 3. Percentage contribution from the Breit interaction to the transition rates. The transitions are from $J = 3/2$ states and the legends are the same as in Fig. 2.

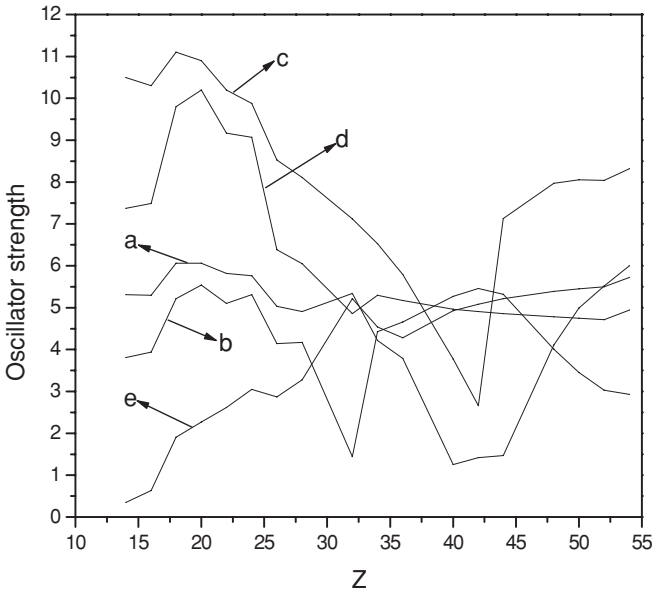

FIG. 4. Weighted oscillator strengths (gf) in powers of 10^{-2} as a function of Z. The curves a, b, c, d, and e correspond to the allowed $1s2s(^3S_1)3p^2P_{1/2}$, $1s2s(^1S_0)3p^2P_{1/2}$, $1s2s(^3S_1)3p^2P_{3/2}$, $1s2s(^1S_0)3p^2P_{3/2}$, and the forbidden $1s2s(^3S_1)3p^4P_{3/2}$ transitions to $1s^22s(^2S_{1/2})$ state, respectively.

and 30.4×10^{13} s^{-1}, respectively. The spin forbidden rates are in excellent agreement with Chen's rates. We believe that the anomaly observed in large configuration mixing for $Z = 42$ leads to transition assignments different from that of Chen [18] thereby resulting in apparent large deviations between ours and Chen's rates.

It is also evident from Table III that the spin-forbidden rates from $^4P_{1/2}$ and $^4P_{3/2}$ states of $1s2s3p$ configuration start as week transition. While the $^4P_{1/2}$–$^2S_{1/2}$ transition remains weak for all the elements considered in this work, the intensity of $^4P_{3/2}$–$^2S_{1/2}$ transition increases rapidly with Z and at $Z = 40$, the intensity of $^4P_{3/2}$–$^2S_{1/2}$ transition equals that of $^2P_{3/2}$–$^2S_{1/2}$ transition from $1s2s(^1S_0)3p$ configuration. Beyond $Z = 40$, the former becomes more intense than the latter and is comparable to that of $(^1S_0)^2P_{1/2}$–$^2S_{1/2}$ transition rate. Also, $^4P_{3/2}$–$^2S_{1/2}$ transition rate is larger than $^2P_{3/2}$–$^2S_{1/2}$ rate from $1s2s(^3S_1)3p$ configurations for $38 \leqslant Z \leqslant 44$. The complex structure arising from mixing of the correlation functions is responsible for the anomalous nature of the spectra for ions in this range.

Our computations show that correlation effect either enhances or reduces the allowed transitions while it enhances the spin rates and its contribution decreases with increasing Z. In Fig. 1, the percentage correlation contribution to the length gauge $E1$ rates of allowed transitions from large expansion set with respect to limited (24 CSFs) set without higher-order corrections are displayed. It is seen from the figure that the correlation effect in general reduces the rates from the $J = 1/2$ and $3/2$ states of the $1s2s(^3S_1)3p$ configurations while it enhances the allowed rates from states of the $1s2s(^1S_0)3p$ configuration. The anomalous trend in the characteristics of correlation contribution is due to mainly to subtle variations in CSFs mixing observed for ions beyond $Z = 38$.

To explore the effect of the Breit interaction on the $E1$ rates, the percentage contributions from the Breit interaction to the length gauge RCI rates of x rays calculated with large multiconfiguration sets are plotted in Figs. 2 and 3 for transitions from the three $J = 1/2$ and $3/2$ states, respectively. It is observed from Figs. 2 and 3 that Breit interaction increases the spin-forbidden rates. While the Breit interaction increases the MCDF rates of $(^3S_1)^2P_{1/2}$–$^2S_{1/2}$ transition, it decreases the other allowed transition rate from $J = 1/2$ state. However, the trend changes somewhere around $Z = 38$ and this change in the Breit contribution is expected to be again due to level crossing. Unlike the Breit contribution to the allowed $E1$ rates from $J = 1/2$ states, we find from Fig. 3 that the influence of the Breit interaction is to reduce the allowed dipole rates from $J = 3/2$ states. Again, the nonsmooth variations in the Breit interaction on the $(^3S_1)^2P_{3/2}$–$^2S_{1/2}$ transition rate is due to anomalous changes in the level scheme.

In Fig. 4 we display the weighted oscillator strengths (gf) for various allowed and the intense $^4P_{3/2}$–$^2S_{1/2}$ transitions. The nonsmooth variations in the oscillator strengths for mid-Z ions are mainly due to the influence of the Breit interaction coupled with correlation.

IV. CONCLUSION

In this work, we have provided a detailed study of the fine-structure states from the $1s2s3p$ configuration in Li-like ions with $Z = 14$ to 54 and reported the allowed and forbidden Kβ satellite x-ray wavelengths, rates, and weighted oscillator strengths. We have, in particular, analyzed the effects of correlations and the Breit interaction on the level energies and x-ray rates. The most striking feature of our work is the sensitivity of subtle changes in the admixture of CSFs on the level scheme and transition rates revealing the unexpected departure from known regularities. We find that additional electron-electron and Breit interactions flip the levels and we note an anomalous structure for mid-Z ions around $Z = 38$. The x rays reported in this work reveal that correlation effects alter significantly the rates more than the energy levels and the contribution from limited configuration mixing is not sufficient to predict the expected rates. The influence of the Breit interaction on the dipole rates varies with the type of transition considered and is Z dependent.

ACKNOWLEDGMENTS

This work was supported by the project Grant No. SR/S2 LOP-10 financed by the Department of Science and Technology, Government of India, New Delhi, India.

[1] K. J. H. Phillips, C. D. Pikes, J. Lang, T. Watanbe, and M. Takahashi, Astrophys. J. **435**, 888 (1994).

[2] V. Desclaux, P. Beiersdofer, S. M. Kahn, and V. L. Jacobs, Astrophys. J. **482**, 1076 (1997).

[3] J. F. Seely, Phys. Rev. Lett. **42**, 1606 (1979).

[4] E. Kallne, J. Kallne, E. S. Marmar, and J. E. Rice, Phys. Scr. **31**, 551 (1985).

[5] V. A. Boiko, A. Ya Faenov, S. A. Pikuz, I. Yu Skobelev, A. V. Vinogradov, and E. A. Yokov, J. Phys. B **10**, 3387 (1977).
[6] P. Beiersdorfer, M. Bitter, S. von Goeler, and K. W. Hill, Phys. Rev. A **40**, 150 (1989).
[7] M. Bitter, H. Hsuan, V. Decaux, B. Grek, K. W. Hill, R. Hulse, L. A. Kruegel, D. Johnson, S. von Goeler, and M. Zarnstorff, Phys. Rev. A **44**, 1796 (1991).
[8] A. J. Smith, M. Bitter, H. Hsuan, K. W. Hill, S. von Goeler, J. Timberlake, P. Beiersdorfer, and A. Osterheld, Phys. Rev. A **47**, 3073 (1993).
[9] P. Beiersdorfer, M. Bitter, D. Hey, and K. J. Reed, Phys. Rev. A **66**, 032504 (2002).
[10] J. E. Rice, M. A. Graf, J. L. Terry, E. S. Marmar, K. Geising, and F. Bombarda, J. Phys. B **28**, 893 (1995).
[11] J. P. Mosnier, R. Barchewitz, M. Cukier, R. Dei-cas, C. Senemaud, and J. Bruneau, J. Phys. B **19**, 2531 (1986).
[12] A. Langenberg, R. L. Watson, and J. R. White, J. Phys. B **13**, 4193 (1980).
[13] M. R. Tarbutt, R. Barnsley, N. J. Peacock, and J. D. Silven, J. Phys. B **34**, 3979 (2001).
[14] A. J. Smith, P. Beiersdorfer, K. J. Reed, A. L. Osterheld, V. Decaux, K. Widmann, and M. H. Chen Phys. Rev. A **62**, 012704 (2000).
[15] S. R. Elliott, P. Beiersdorfer, S. B. Libby, A. L. Osterheld, and T. Phillips, Optic Communications **113**, 204 (1994).
[16] K. J. H Phillips, J. Dubau, J. Sylwester, and B. Sylwester, Astrophy. J. **638**, 115 (2006).
[17] U. I Safranova, M. S. Safronova, and R. Bruch, J. Phys. B **28**, 2803 (1995).
[18] M. H. Chen, At. Data. Nucl. Data Tables **34**, 301 (1986).
[19] Y. Y. Goryayev, A. M. Urnov, and L. A. Vainshtein, e-print arXiv:physics/0603164v 2, 3 April 2006.
[20] L. Natarajan and Anuradha Natarajan, Phys. Rev A **79**, 062513 (2009).
[21] L. Natarjan and Anuradha Natarjan, Phys. Rev. A **75**, 062502 (2007).
[22] C. Froesce Fischer, T. Brage, and P. Jonnson, *Computational Atomic Structure* (IOP, Bristol, 1997).
[23] P. Jonsson, X. He, C. Froese Fischer, and I. P. Grant, Comput. Phys. Commun. **177**, 597 (2007).
[24] I. P. Grant, B. J. McKenzie, P. H. Norrington, D. F. Mayers, and N. C. Pyper, Comput. Phys. Commun. **21**, 207 (1980).
[25] K. G. Dyall, I. P. Grant, C. T. Johnson, F. A. Parpia, and E. P. Plummer, Comput. Phys. Commun. **55**, 425 (1989).
[26] Y.-K. Kim, D. H. Baik, P. Indelicato, and J. P. Desclaux, Phys. Rev. A **44**, 148 (1991).
[27] Anuradha Natarajan and L. Natarajan, J. Phys. B **37**, 4789 (2004).
[28] Anuradha Natarajan and L. Natarajan, J. Quant. Spectrosc. Radiat. Transf. **109**, 2281 (2008).